Neurobiology of Disease

Differential Vulnerability of CA1 versus CA3 Pyramidal Neurons After Ischemia: Possible Relationship to Sources of Zn^{2+} Accumulation and Its Entry into and Prolonged Effects on Mitochondria

Yuliya V. Medvedeva,[1] **Sung G. Ji,**[2] **Hong Z. Yin,**[1] **and John H. Weiss**[1]

[1]Department of Neurology and [2]Department of Anatomy and Neurobiology, University of California, Irvine, California 92697

Excitotoxic mechanisms contribute to the degeneration of hippocampal pyramidal neurons after recurrent seizures and brain ischemia. However, susceptibility differs, with CA1 neurons degenerating preferentially after global ischemia and CA3 neurons after limbic seizures. Whereas most studies address contributions of excitotoxic Ca^{2+} entry, it is apparent that Zn^{2+} also contributes, reflecting accumulation in neurons either after synaptic release and entry through postsynaptic channels or upon mobilization from intracellular Zn^{2+}-binding proteins such as metallothionein-III (MT-III). Using mouse hippocampal slices to study acute oxygen glucose deprivation (OGD)-triggered neurodegeneration, we found evidence for early contributions of excitotoxic Ca^{2+} and Zn^{2+} accumulation in both CA1 and CA3, as indicated by the ability of Zn^{2+} chelators or Ca^{2+} entry blockers to delay pyramidal neuronal death in both regions. However, using knock-out animals (of MT-III and vesicular Zn^{2+} transporter, ZnT3) and channel blockers revealed substantial differences in relevant Zn^{2+} sources, with critical contributions of presynaptic release and its permeation through Ca^{2+}- (and Zn^{2+})-permeable AMPA channels in CA3 and Zn^{2+} mobilization from MT-III predominating in CA1. To assess the consequences of the intracellular Zn^{2+} accumulation, we used OGD exposures slightly shorter than those causing acute neuronal death; under these conditions, cytosolic Zn^{2+} rises persisted for 10 –30 min after OGD, followed by recovery over ~40 – 60 min. Furthermore, the recovery appeared to be accompanied by mitochondrial Zn^{2+} accumulation (via the mitochondrial Ca^{2+} uniporter MCU) in CA1 but not in CA3 neurons and was markedly diminished in MT-III knock-outs, suggesting that it depended upon Zn^{2+} mobilization from this protein.

Key words: CA1 pyramidal neurons; delayed degeneration; hippocampal slice; *in vitro* ischemia model; mitochondria; oxygen glucose deprivation

Significance Statement

The basis for the differential vulnerabilities of CA1 versus CA3 pyramidal neurons is unclear. The present study of events during and after acute oxygen glucose deprivation highlights a possible important difference, with rapid synaptic entry of Ca^{2+} and Zn^{2+} contributing more in CA3, but with delayed and long-lasting accumulation of Zn^{2+} within mitochondria occurring in CA1 but not CA3 pyramidal neurons. These data may be consistent with observations of prominent mitochondrial dysfunction as a critical early event in the delayed degeneration of CA1 neurons after ischemia and support a hypothesis that mitochondrial Zn^{2+} accumulation in the early reperfusion period may be a critical and targetable upstream event in the injury cascade.

Introduction

Hippocampal pyramidal neurons (HPNs) of the CA1 and CA3 domains are highly vulnerable to injury in pathological conditions of prolonged or recurrent seizures or after brain ischemia. However, their patterns of vulnerability differ, likely reflecting differences in events leading to their degeneration. CA3 neurons are preferentially lost in response to limbic seizures occurring after kainic acid injection into the amygdala (Ben-Ari et al.,

Received Oct. 22, 2016; revised Nov. 23, 2016; accepted Nov. 29, 2016.

Author contributions: Y.V.M., S.G.J., and J.H.W. designed research; Y.V.M., S.G.J., and H.Z.Y. performed research; Y.V.M. and S.G.J. analyzed data; Y.V.M. and J.H.W. wrote the paper.

This work was supported by the National Institutes of Health (Grants NS065219 and NS096987 to J.H.W.). We thank Edward Sharman for editorial assistance and helpful discussions.

The authors declare no competing financial interests.

Correspondence should be addressed to J.H. Weiss, MD, Ph.D., Department of Neurology, University of California, 2101 Gillespie Bldg., Irvine, CA 92697-4299. E-mail: **jweiss@uci.edu**.

DOI:10.1523/JNEUROSCI.3270-16.2016

Copyright © 2017 the authors 0270-6474/17/370726-12$15.00/0

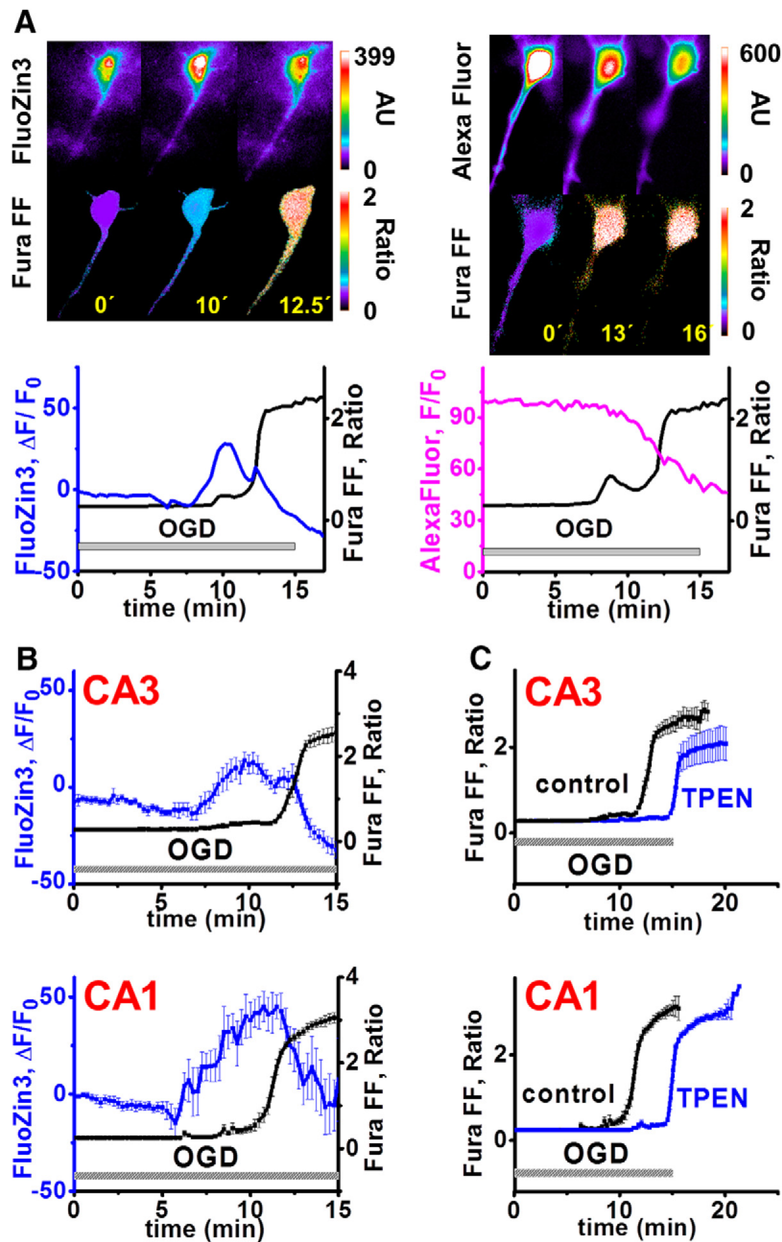

Figure 1. OGD-evoked Zn^{2+} rises precede and contribute to Ca^{2+} deregulation in both CA3 and CA1 pyramidal neurons. ***A***, Relationship between intracellular Zn^{2+} and Ca^{2+} rises and loss of membrane integrity in individual CA3 neurons subjected to OGD. Pseudocolor fluorescent images (top) show cells loaded with a low-affinity ratiometric Ca^{2+} indicator (Fura-FF; 340/380 ratio images), along with either a Zn^{2+}-sensitive indicator (FluoZin-3, background subtracted emission intensity, arbitrary units, AU; left) or an ion-insensitive fluorescent compound (Alexa Fluor-488, background-subtracted emission intensity, AU; right) and subjected to 15 min of OGD. Numbers indicate time (in minutes) after the onset of OGD. Traces (bottom) show fluorescence changes in the same neurons. Note that the Zn^{2+} rise precedes a sharp Ca^{2+} deregulation event (left) and that the Ca^{2+} deregulation is accompanied by a loss of the Alexa Fluor-488 signal (one cell representative of four; right), indicative of loss of membrane integrity. ***B***, Zn^{2+} rises precede the terminal Ca^{2+} deregulation in CA3 as well as CA1 pyramidal neurons. Individual FluoZin-3- and Fura-FF-loaded CA1 and CA3 neurons were subjected to OGD; traces (±SEM; aligned for the onset of Ca^{2+} deregulation) show mean changes in somatic FluoZin-3 fluorescence ($\Delta F/F_o$; blue) and Fura-FF ratio changes (black; CA3, top: Zn^{2+} rise 7.7 ± 0.6 min, Ca^{2+} rise 11.6 ± 0.6 min, $n = 8$, $p = 5.1 \times 10^{-4}$; CA1, bottom: Zn^{2+} rise 7.5 ± 0.5 min, Ca^{2+} rise 10.6 ± 0.5 min; $n = 9$, $p = 3.4 \times 10^{-4}$; the interval from the Zn^{2+} rise to the Ca^{2+} deregulation was not different between CA1 and CA3; $p = 0.452$, ANOVA linear contrast). ***C***, Similar Zn^{2+} contributions to the occurrence of terminal Ca^{2+} deregulation in CA3 and CA1 pyramidal neurons. Hippocampal slices were subjected to OGD alone (black) or in the presence of the Zn^{2+} chelator TPEN (40 μM; blue). Traces (±SEM; aligned for the onset of Ca^{2+} deregulation) show mean Fura-FF ratio changes (CA3, top: control: 11.2 ± 0.7 min, $n = 9$; TPEN: 14.4 ± 0.6 min, $n = 6$, $p = 5.3 \times 10^{-3}$; CA1, bottom: control: 10.6 ± 0.5 min, $n = 9$; TPEN: 14.7 ± 0.7 min, $n = 9$, $p = 1.1 \times 10^{-4}$; TPEN-induced delay in Ca^{2+} deregulation was not different between CA3 and CA1, $p = 0.62$, ANOVA linear contrast).

1980a; Ben-Ari et al., 1980b; Tanaka et al., 1988). In contrast, delayed selective degeneration of CA1 neurons is conspicuous after transient ischemia in humans (Zola-Morgan et al., 1986; Petito et al., 1987) and rodents (Kirino, 1982; Ordy et al., 1993; Sugawara et al., 1999).

Excitotoxic mechanisms caused by excessive glutamate release have long been considered important contributors to ischemic neurodegeneration. Most studies have focused upon the role of rapid Ca^{2+} entry through NMDA-type glutamate receptors. Indeed, glutamate-triggered injury to cultured neurons is Ca^{2+} dependent (Choi, 1987) and delayed sharp Ca^{2+} rises occurring after the end of the glutamate exposures are indicative of cell death (Rothman and Olney, 1986; Siesjö, 1988; Randall and Thayer, 1992). However, despite intense early interest, research into the clinical efficacy of glutamate antagonists has been limited.

Further studies have highlighted contributions of another divalent cation, Zn^{2+}, which is present in the brain at high levels, accumulates in HPNs after ischemia or prolonged seizures, and has been implicated in ischemic neurodegeneration (Frederickson et al., 1989; Tønder et al., 1990; Koh et al., 1996; Yin et al., 2002; Calderone et al., 2004). It is apparent that there are two distinct sources of the Zn^{2+} that accumulate in neurons after ischemia or prolonged seizures. One comprises presynaptic vesicular Zn^{2+} that is released and enters the postsynaptic neurons ("translocation"), likely in large part through highly Ca^{2+}-permeable AMPA (Ca-AMPA) channels (which are also highly Zn^{2+} permeable) (Yin et al., 2002; Calderone et al., 2004; Noh et al., 2005). In addition, Zn^{2+} can be released from cytosolic buffering proteins such as metallothioneins (MTs) already present in the neurons (Aizenman et al., 2000; Lee et al., 2000; Lee et al., 2003).

Early effects of ischemia can be studied in brain slices subjected to oxygen–glucose deprivation (OGD), a procedure that mimics some aspects of stroke. Hippocampal slice models have revealed Zn^{2+} rises to begin shortly after OGD onset and to contribute to subsequent injury (Yin et al., 2002; Wei et al., 2004; Stork and Li, 2006). To discriminate the early effects of Zn^{2+} from those of Ca^{2+}, we tracked these ions simultaneously in CA1 pyramidal neurons in acute hippocampal slices subjected to OGD. We found the Zn^{2+} rises preceded and contributed to the induction of the terminal sharp Ca^{2+} rises ("Ca deregulations"), which were linked causatively to a loss of membrane

integrity (Medvedeva et al., 2009). The early Zn^{2+} rises resulted in mitochondrial accumulation (via the mitochondrial Ca^{2+} uniporter MCU), contributing to their dysfunction and reactive oxygen species (ROS) generation (Medvedeva and Weiss, 2014).

The present slice studies show that Zn^{2+} clearly contributes to acute OGD-induced injury in both CA1 and CA3 neurons and sought to examine differences in early events between these neuronal populations that may bear upon their differential vulnerabilities. Our findings suggest that presynaptic Zn^{2+} release and entry through Ca-AMPA channels dominates in CA3, whereas Zn^{2+} mobilization from MT-III is of greater importance in CA1. Furthermore, when we performed OGD exposures just short of those that induce acute cell death, there was substantial ongoing Zn^{2+} accumulation in mitochondria of CA1 (but not in CA3) neurons that persisted for at least ~30 min after OGD. These findings support the hypothesis that delayed mitochondrial Zn^{2+} accumulation might be a critical trigger of mitochondrial dysfunction and selective degeneration of CA1 pyramidal neurons after transient ischemia. As the Zn^{2+} accumulation progresses during the early postischemic period, delivery of appropriate therapeutics during this period may have the potential to provide substantial benefit.

Materials and Methods

Animals. All procedures were performed according to a protocol approved by the University of California–Irvine Animal Care and Use Committee. Efforts were made to minimize animal suffering and the number of mice used. Three strains of mice of either sex were used for experiments: wild-type mice 129S6/SvEvTac (Taconic Biosciences), mice lacking metallothionein III (004649−129S7-Mt3^{tm1Rpa}/J; Jackson Laboratory) and mice lacking vesicular Zn^{2+} transporter (005064-B6;129-Slc30a3^{tm1Rpa}/J; Jackson Laboratory). The strain of origin for both of these knock-outs is 129S7/SvEvBrd-Hprt<+>. We have characterized the occurrence of OGD-induced Zn^{2+} rises and Ca^{2+} deregulation in each of these knock-out strains and found that Zn^{2+} rises precede Ca^{2+} deregulation in both CA1 and CA3 in both of these strains much as in the WT mice, with no evidence for any generalized differences in viability. The small deviations noted from WT occur in opposite directions in CA1 and CA3 neurons and, in all cases, were explainable based upon prior studies and expectations of the roles of the deleted peptides (MT-III or ZnT3; data not shown). However, despite the reasonable match between these strains, we cannot rule out the possibility of functionally significant differences and thus only make statistical comparisons between responses within the same strain.

Preparation of acute hippocampal slices. Hippocampal slices were prepared from ~4-week-old mice as described previously (Medvedeva et al., 2009). Mice were deeply anesthetized with isoflurane and decapitated and the brains rapidly removed and placed in ice-cold preparation solution containing the following (in mM): sucrose 220, KCl 3, NaH_2PO_4 1.25, $MgSO_4$ 6, $NaHCO_3$ 26, $CaCl_2$ 0.2, glucose 10, and ketamine 0.42, pH 7.35, 310 mOsm equilibrated with 95% O_2/5% CO_2. Hippocampal slices (300 μm) were cut with a vibratome (Leica VT1200) and placed in artificial CSF (ACSF) containing the following (in mM): NaCl 126, KCl 3, NaH_2PO_4 1.25, $MgSO_4$ 1, $NaHCO_3$ 26, $CaCl_2$ 2, glucose 10, pH 7.35, 310 mOsm adjusted with sucrose and equilibrated with 95% O_2/5% CO_2. After equilibration for 1 h at 34 ± 0.5°C, slices were kept at room temperature (20–23°C) in oxygenated ACSF for at least 1 h before use.

Loading individual hippocampal neurons with fluorescent indicators. For recordings, slices were placed in a flow-through chamber (RC-27L chamber with plastic slice anchor; Warner Instruments) mounted on the stage of an upright microscope (BX51WI; Olympus) and perfused with oxygenated ACSF at 2 ml/min. Experiments were performed at 32 ± 0.5°C. Fura-FF, FluoZin-3, or Alexa Fluor-488 were dissolved in a pipette solution containing the following (in mM): 125 K gluconate, 10 KCl, 3 Mg-ATP, 1 $MgCl_2$, 10 HEPES, pH 7.25 with KOH, 290 mOsm with sucrose, at concentrations of 1, 1, and 0.25 mM respectively, and 1 μl placed in the tip of a micropipette (5–7 MΩ, borosilicate glass with filament) before backfilling with pipette solution. Neurons were loaded with fluorescent indicators via patch pipettes by holding them in the whole-cell configuration at −60 mV for 5 min, as described previously (Medvedeva et al., 2009). During pipette withdrawal, cells were monitored to assess membrane leakage and Ca^{2+} levels; intact cells were left to recover for 20 min before starting the experiment.

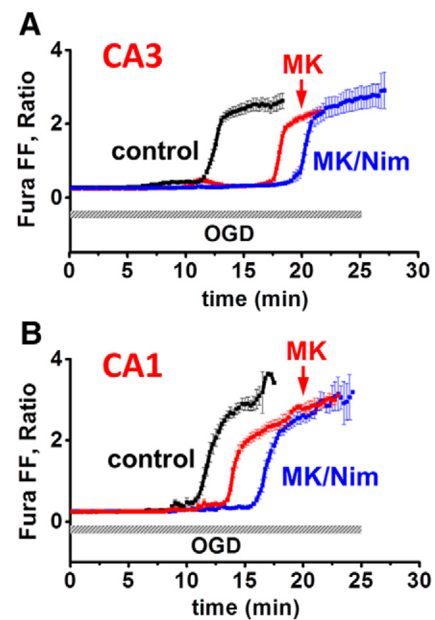

Figure 2. There was a greater contribution of acute NMDA- and VGCC-mediated excitotoxicity to OGD-evoked Ca^{2+} deregulation in CA3 than in CA1 pyramidal neurons. CA1 and CA3 neurons were loaded with FluoZin-3 and Fura-FF and subjected to OGD alone (black), with the NMDA receptor antagonist MK-801 (MK, red; 10 μM), or with both MK-801 and the VGCC blocker nimodipine (MK/Nim, blue; both at 10 μM); traces (±SEM; aligned for the onset of Ca^{2+} deregulation) show mean Fura-FF ratio changes. Each of these anti-excitotoxic interventions delayed Ca^{2+} deregulation in both CA3 (***A***) and CA1 (***B***) (CA3: control: 11.1 ± 0.6, $n = 13$; MK-801: 17.5 ± 0.5, $n = 5$, $p = 5.7 \times 10^{-6}$; MK/Nim: 20.2 ± 0.9 min, $n = 10$, $p = 7.8 \times 10^{-9}$ vs control for both treatments; CA1: control: 10.6 ± 0.5 min, $n = 9$; MK-801: 13.5 ± 1.1 min, $n = 7$, $p = 0.017$; MK/Nim: 16.7 ± 0.8 min, $n = 10$, $p = 1.4 \times 10^{-5}$ vs control). Notably, each of these interventions provided a greater degree of protection in CA3 than in CA1 ($p = 0.044$ for MK801 alone and $p = 0.019$ for MK/Nim by ANOVA linear contrast).

Fluorescent measurements. For simultaneous measurements of intracellular Ca^{2+} and Zn^{2+} dynamics, cells were coloaded with a low-affinity Ca^{2+} indicator (Fura-FF, K_d ~ 5.5 μM) and a high-affinity Zn^{2+} indicator FluoZin-3 (K_d ~ 15 nM). To assess changes in membrane integrity, the ion-insensitive fluorescent compound Alexa Fluor-488 was coloaded with Fura-FF. Fluorescence was alternately excited at 340(20), 380(20), and 482(20) nm via a 40× water-immersion objective using a xenon light source (Sutter Instruments) and emitted fluorescence was collected at 532 (40) nm using a cooled CCD camera (Hamamatsu) (All filters are band pass with bandwidths indicated in parentheses.) Images were acquired every 15 or 30 s, background subtracted, and analyzed using METAFLUOR version 7.1 software (Universal Imaging). Changes in Ca^{2+} values are presented as the ratio of background subtracted Fura-FF emission intensities upon excitation at 340 and 380 nm ("340/380 ratio"), FluoZin-3 fluorescence changes as $\Delta F/F_0 = (F - F_0)/F_0$, and Alexa Fluor-488 fluorescence changes as F/F_0, where F is the current fluorescence intensity and F_0 is the average background-subtracted baseline fluorescence during the 10 min before OGD.

To assess changes in mitochondrial potential ($\Delta\Psi_m$), slices were bulk loaded with the $\Delta\Psi_m$-sensitive indicator rhodamine 123 (Rhod123, 26 μM, 30 min, 20–23°C). Rhod123 is positively charged and accumulates in negatively charged mitochondria, where its fluorescence is quenched. Upon mitochondrial depolarization, it is released into the cytoplasm, causing an increase in fluorescence (Duchen et al., 2003). Rhod123 was excited at 540 (25) nm and emitted fluorescence collected at 605 (55) nm.

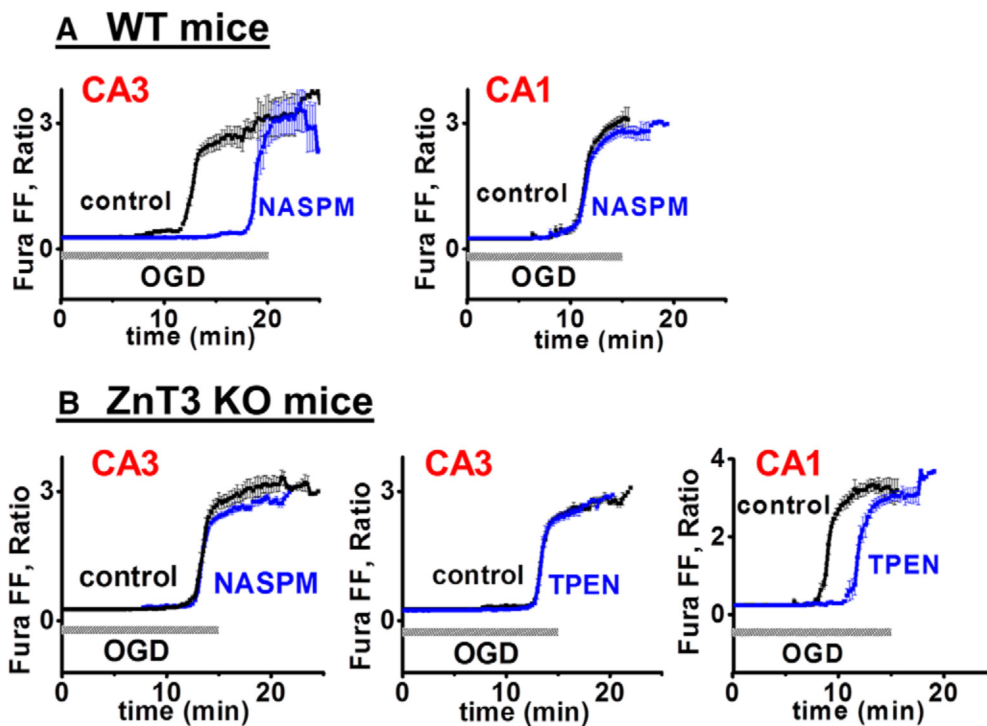

Figure 3. Contribution of synaptic Zn^{2+} release and its entry through Ca-AMPA channels to OGD-evoked Ca^{2+} deregulation in CA3 pyramidal neurons. CA1 and CA3 neurons in slices from wild-type mice (***A***) and ZnT3 KO mice (***B***) were loaded with Fura-FF and FluoZin-3 and subjected to OGD alone (black) or in the presence of TPEN (40 μM) or NASPM (100 μM) as indicated (blue). Traces ($\pm$SEM; aligned for the onset of Ca^{2+} deregulation) show mean Fura-FF ratio changes. ***A***, Ca-AMPA channel blockade substantially delays Ca^{2+} deregulation in CA3 (left), with no effect on CA1 neurons (right) (CA3: control: 11.5 $\pm$ 0.7 min, $n = 7$; NASPM: 18.1 $\pm$ 1.2 min, $n = 5$; $p = 6 \times 10^{-4}$; CA1: control: 10.6 $\pm$ 0.5 min, $n = 9$; NASPM: 10.7 $\pm$ 0.4 min, $n = 5$; $p = 0.86$). ***B***, In the absence of vesicular Zn^{2+} (in ZnT3 KOs), the protective effects of TPEN and of NASPM on CA3 neurons are eliminated (but TPEN still protects in CA1; CA3: control: 12.1 $\pm$ 0.9 min, $n = 9$; NASPM: 12.8 $\pm$ 0.9 min, $n = 9$, $p = 0.58$; TPEN: 12.2 $\pm$ 0.6 min, $n = 6$, $p = 0.96$; CA1: control: 8.4 $\pm$ 0.8 min, $n = 6$; TPEN: 11.5 $\pm$ 1.0 min, $n = 7$, $p = 0.037$).

Images were acquired every 15 s and data presented as $\Delta F/F_0 = (F - F_0)/F_0$ where F is a current fluorescence intensity and F_0 is the fluorescence intensity in the resting slice. Regions of interest were monitored in the CA1 or CA3 pyramidal cell layers.

OGD in slices. To simulate hypoxic–hypoglycemic conditions, ACSF was changed to identical solution lacking glucose and bubbled with 95% N_2/5% CO_2. In studies examining acute OGD-induced neurodegeneration, OGD was continued for at least 15 min and maintained throughout the time of the terminal Ca^{2+} deregulation. For sublethal OGD exposures, OGD was terminated (by restoration of oxygenated ACSF) ~1 min after start of the Zn^{2+} rise in experiments in which Zn^{2+} was measured (typically occurring from 6–9 min), or, for the Rhod123 (see Fig. 5) and confocal imaging (see Fig. 7) studies, after 8.5–9 min as indicated.

MK-801 (10 μM), nimodipine (10 μM), 1-naphthyl acetyl spermine (NASPM, 100 μM) and N,N,N′,N′-tetrakis(2-pyridylmethyl)ethane-1,2-diamine (TPEN, 40 μM) were applied 10 min before and during OGD. Ruthenium Red (RR) (10 μM) and carbonyl cyanide-4-(trifluoromethoxy)phenylhydrazone (FCCP, 2 μM) were applied after the termination of OGD as indicated.

Antibody labeling and confocal microscopy. Hippocampal slices (300 μm) were subjected to OGD as described above for 8.5 min, "perfused" in ACSF at 32°C for 1 h, and immediately fixed with 4% paraformaldehyde. Thin (30 μm) sections were cut using a microtome cryostat (ThermoFisher Scientific) and stained with primary antibodies against the mitochondrial outer membrane protein TOM20 (1:200; Santa Cruz Biotechnology) and secondary anti-rabbit fluorescent antibodies (1:200, DyLight 488; Jackson ImmunoResearch). The sections were imaged using an inverted stage Nikon Eclipse Ti chassis microscope with a Yokogawa CSUX spinning disk head and a 100× (1.49 numerical aperture) objective and images acquired using a Hamamatsu electromultiplying CCD camera. Excitation (488 nm) was via a Coherent sapphire laser source synchronized with the camera, emission was monitored with a 525 (50) nm filter, and images were acquired using MIcroManager ImageAcquisition sofrware (version 1.4.16). Bright-field images were obtained using the same objective at the same z-axis position immediately after acquiring the fluorescent image.

For analysis of mitochondria size and shape (using ImageJ software), we selected large neurons in the pyramidal cell layer. To control for differing behavior of mitochondria between distinct cell types and cellular compartments, we chose to focus our studies on mitochondria surrounding the prominent nucleii of pyramidal neurons and selected fields for analysis in which mitochondria were clearly evident in perinuclear regions in the plane of sharp focus. Images were adjusted to provide optimal discrimination of their apparent edges from background. In the perinuclear regions, mitochondria are aligned with their long axes parallel to the nuclear membrane. Nuclear regions in which clearly demarcated mitochondria were evident were cropped from images and saved with a code name for blinded measurements and measures of long axes parallel to and short axes perpendicular to nuclear membranes were obtained on all clearly demarcated mitochondria adjacent to and surrounding the nuclear circumference. Mean parameters were determined for mitochondria within each cell, the cell values were averaged to determine the mean paramaters within each independent slice, and presented values are means from three to five slices for each condition.

Reagents. Fura-FF, FluorZin-3, Rhodamine 123, and Alexa Fluor-488 hydrazide were from Invitrogen. MK-801 was from Abcam, TPEN, RR, and ketamine were from Sigma-Aldrich. Nimodipine was from Miles. NASPM was from Tocris Bioscience. TOM20 antibodies were from Santa Cruz Biotechnology (catalog #sc-11415, *RRID*:AB_2207533) and DyLight 488 antibodies were from Jackson ImmunoResearch (catalog #211-482-171). All other reagents were purchased from Fisher Scientific.

Statistics and data analysis. The onset times of OGD-induced Zn^{2+} rises and of Ca^{2+} deregulations were determined by finding intersections between the extrapolated baselines, with lines fitting the first substantial FluoZin-3 fluorescence increases or Fura-FF ratio increases, as described previously (Medvedeva et al., 2009). Differences between sets of data

were assessed using two-sample *t* tests (Origin 9.1). In some studies, we sought to determine whether the degree of protection provided by an intervention (assessed as the mean interval between the time of Ca^{2+} deregulation in control and treatment groups) or the interval between the Zn^{2+} rise and the Ca^{2+} deregulation differed between CA1 and CA3 neurons. For these assessments, we used the ANOVA linear contrast test (STATA software). All comparisons reflect sets of data substantially interleaved in time and were based on five to 10 slices from at least five animals for each condition (numbers of cells and slices are indicated for each experiment). All values are presented as means ± SEM.

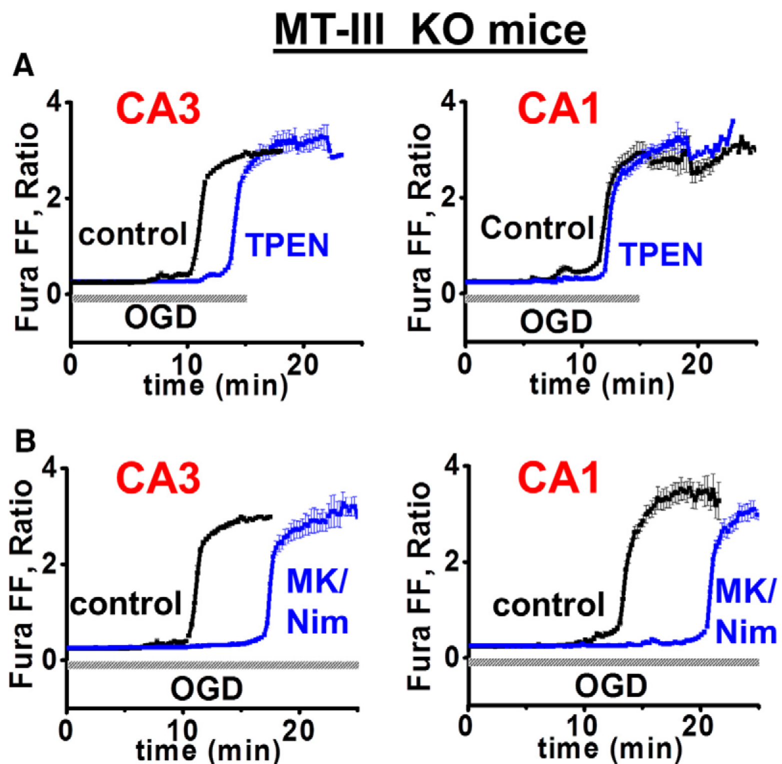

Figure 4. MT-III deletion substantially eliminates the Zn^{2+} contribution to acute OGD-induced injury in CA1 (but not CA3) pyramidal neurons. CA1 and CA3 neurons in slices from MT-III KO mice were loaded with Fura-FF and FluoZin-3 and subjected to OGD alone (black) or with either TPEN (40 μM) or MK-801+ nimodipine (MK/Nim, each at 10 μM) as indicated (blue). Traces (±SEM; aligned for the onset of Ca^{2+} deregulation) show mean Fura-FF ratio changes. ***A***, In the absence of MT-III, the protective effects of TPEN persist in CA3 (left) but are eliminated in CA1 (right) (CA3: control: 10.2 ± 0.7 min, $n = 8$, TPEN: 13.6 ± 0.7 min, $n = 8$, $p = 3.7 \times 10^{-3}$; CA1: control: 11.6 ± 0.7 min, $n = 9$, TPEN: 12.0 ± 0.8 min, $n = 7$, $p = 0.76$). ***B***, In the absence of MT-III, NMDA- and VGCC-mediated excitotoxicity contributes substantially to OGD-evoked Ca^{2+} deregulation in both CA3 and CA1 pyramidal neurons (CA3: control: 10.2 ± 0.7 min, $n = 8$, MK/Nim: 17.2 ± 1.2 min, $n = 7$, $p = 5.2 \times 10^{-4}$; CA1: control: 13.0 ± 0.7 min, $n = 9$, MK/Nim: 20.4 ± 0.7 min, $n = 10$, $p = 3.1 \times 10^{-7}$; the MK/Nim-induced delay in Ca^{2+} deregulation was not different between CA3 and CA1, $p = 0.78$, ANOVA linear contrast).

Results

Ca^{2+} and Zn^{2+} contribute to OGD-induced degeneration of both CA3 and CA1 pyramidal neurons

In recent studies (Medvedeva et al., 2009; Medvedeva and Weiss, 2014), we examined Ca^{2+} and Zn^{2+} changes in hippocampal CA1 pyramidal neurons during acute OGD and their respective contributions to neuronal injury. When the slices were subjected to OGD, we found that cytosolic Zn^{2+} rises began within several minutes and preceded very high cytosolic Ca^{2+} rises (termed "Ca^{2+} deregulation" events), which were terminal events because they were accompanied by a loss of membrane integrity. These Ca^{2+} deregulations were delayed by the addition of the high-affinity Zn^{2+} chelator TPEN, indicating a contribution of the Zn^{2+} to the cell death cascade.

Because there are likely to be therapeutically significant differences in the sequence of events linking ischemia to degeneration of CA1 versus CA3 neurons, we used the same paradigm to examine the contribution of Zn^{2+} and Ca^{2+} in acute ischemic degeneration of CA3 neurons. As in our prior studies, single neurons in acute slices were coloaded with membrane impermeable forms of the high-affinity Zn^{2+} indicator FluoZin-3 (K_d ~15 nM) and the low-affinity ratiometric Ca^{2+} indicator Fura-FF (K_d ~5.5 μM) via a patch pipette and the slices were subjected to OGD as described previously (Medvedeva et al., 2009; Medvedeva and Weiss, 2014; see Materials and Methods) while monitoring changes in cytosolic Zn^{2+} (as $\Delta F/F_0$) and Ca^{2+} (as 340/380 ratio). We found that, as in CA1, Zn^{2+} rises preceded Ca^{2+} deregulation events in CA3 (Fig. 1*A*,*B*).

To confirm that the Ca^{2+} deregulations were terminal events in CA3, other neurons were coloaded with the low-affinity Ca^{2+} indicator Fura-FF, along with the ion-insensitive fluorescent compound Alexa Fluor-488. As in CA1 (Medvedeva et al., 2009), Ca^{2+} deregulation was always accompanied by the onset of a dramatic loss of Alexa Fluor-488 fluorescence in the absence of any recovery of the cytosolic Ca^{2+}, indicating a terminal loss of membrane integrity (Randall and Thayer, 1992; Vander Jagt et al., 2008; Fig. 1*A*). Furthermore, the Ca^{2+} deregulation in CA3 pyramidal neurons was delayed by Zn^{2+} chelation (with TPEN, 40 μM) to a similar degree as in CA1 (Fig. 1*C*), indicating that Zn^{2+} contributes to the onset of this terminal event in both subfields.

'Excitotoxicity' contributes to OGD-induced degeneration in both CA3 and CA1 pyramidal neurons

Most studies of acute excitotoxicity have focused upon the contribution of rapid Ca^{2+} entry through highly Ca^{2+}-permeable NMDA-receptor-gated channels. Ca^{2+} can also enter depolarized neurons via voltage-gated Ca^{2+} channels (VGCCs). To assess the contribution of these Ca^{2+} entry routes to OGD induced degeneration, we tested effects of the NMDA blocker MK-801 alone or in the additional presence of the VGCC blocker nimodipine (each at 10 μM added 10 min before start of OGD). Each of these treatments delayed Ca^{2+} deregulation in both CA3 and CA1 neurons. Interestingly, each of these treatments provided significantly greater protection in CA3 than in CA1, suggesting a greater acute excitotoxic contribution to ischemic injury in CA3 (Fig. 2), possibly consistent with the greater susceptibility of CA3 neurons to recurrent limbic seizures.

Critical contribution of Zn^{2+} entry through Ca-AMPA to acute OGD injury in CA3

AMPA-type glutamate receptors, which mediate most rapid excitatory neurotransmission, are tetramers composed of combinations of four subunits (GluA1–4). Whereas most AMPA

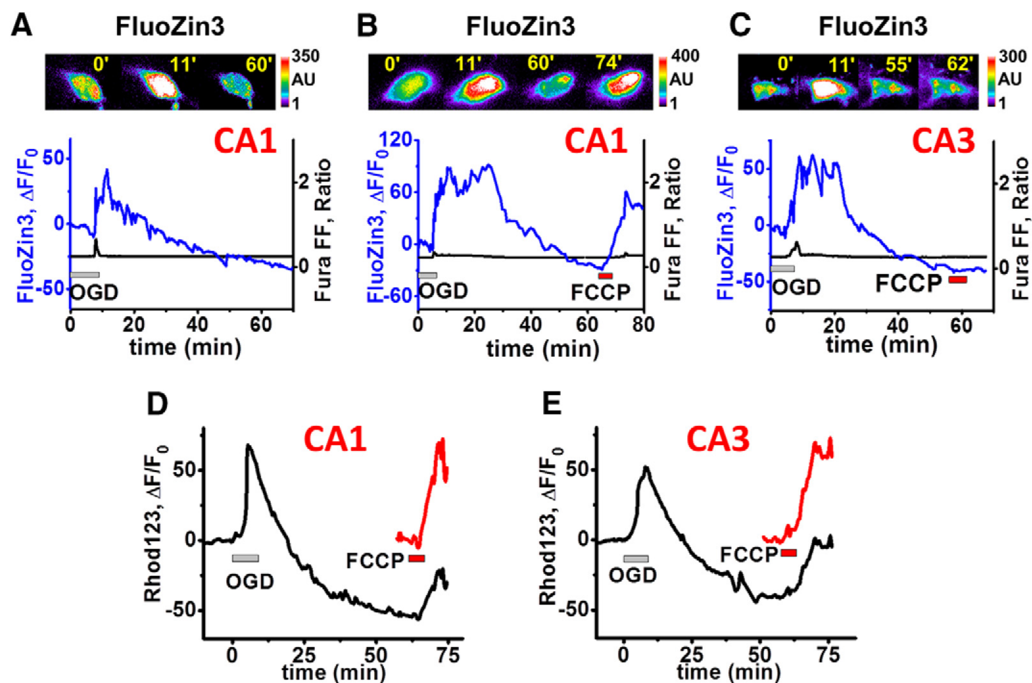

Figure 5. Sublethal OGD evokes delayed mitochondrial Zn^{2+} accumulation in CA1, but not in CA3 pyramidal neurons. ***A–C***, Individual CA1 and CA3 neurons in slices from wild-type mice were loaded with Fura-FF and FluoZin-3, subjected to sublethal episodes of OGD (~7–10 min, OGD terminated ~1 min after the initial cytosolic Zn^{2+} rise) and cytosolic Zn^{2+} (monitored as FluoZin-3 $\Delta F/F_0$), and followed for an additional hour without (***A***) or with (***B***, ***C***) the delayed addition of FCCP (2 μM × 5 min, as indicated). Pseudocolor images show FluoZin-3 fluorescence in single representative neurons at the indicated times after the start of OGD (in minutes), and traces (FluoZin-3 $\Delta F/F_0$, blue; Fura-FF ratio, black) show time course of changes in the same neurons (mean start times of the initial OGD-evoked Zn^{2+} rise were as follows: ***A***: 8.0 ± 0.8 min, $n = 5$; ***B***: 7.7 ± 0.75 min, $n = 7$; and ***C***: 7.2 ± 0.38 min, $n = 8$ neurons). ***A***, Cytosolic Zn^{2+} rise and slow recovery in CA1 neurons after sublethal OGD. Note the further rise after the termination of OGD followed by a slow recovery of cytosolic Zn^{2+} over the ~30 min after the OGD (trace representative of $n = 5$). ***B***, ***C***, Administration of FCCP 55–60 min after OGD termination evoked large cytosolic Zn^{2+} rises in CA1 but not in CA3 neurons (mean FCCP elicited Zn^{2+} rises at 55–60 min: CA1: 75 ± 21.9%, $n = 7$; CA3: 8.75 ± 7.4%, $n = 8$, $p = 3.5 \times 10^{-3}$). ***D***, ***E***, Substantial recovery of mitochondrial potential ($\Delta\Psi_m$) in both CA1 and CA3 pyramidal neurons after sublethal OGD. Slices were bath loaded with Rhod123 and subjected to sublethal (9 min) OGD followed after ~50 min by FCCP application as indicated. Traces (from representative single neurons) demonstrate changes in Rhod123 fluorescence relative to the pre-OGD baseline (ΔF_{OGD}). However, because slow dye loss from the slices after OGD attenuated absolute ΔF rises, for quantitative comparisons of magnitudes of ΔF changes (reflecting the degree of $\Delta\Psi$m loss triggered by OGD vs that triggered by FCCP), responses were renormalized to the 3 min just before the addition of FCCP (ΔF_{FCCP}; red; CA1: ΔF_{OGD} 63 ± 5.7%, ΔF_{FCCP} 58.7 ± 5.2%, $\Delta F_{FCCP}/\Delta F_{OGD}$ 0.98 ± 0.14, $n = 6$; CA3: ΔF_{OGD} 56 ± 3.5%, ΔF_{FCCP} 56 ± 10%, $\Delta F_{FCCP}/\Delta F_{OGD}$ 1.02 ± 0.19, $n = 7$; $p = 0.88$).

channels are Ca^{2+} impermeable, those lacking the GluA2 subunit are Ca^{2+} permeable (Ca-AMPA channels; Hollmann et al., 1991; Verdoorn et al., 1991). Although it was originally thought that pyramidal neurons express few Ca-AMPA channels, it later became apparent that they are present at variable levels on many pyramidal neurons and may be found preferentially in dendritic membranes adjacent to sites of presynaptic glutamate release (Lerma et al., 1994; Yin et al., 1999; Ogoshi and Weiss, 2003). In addition to being Ca^{2+} permeable, these channels, unlike NMDA channels, are also highly permeable to Zn^{2+} (Yin and Weiss, 1995; Sensi et al., 1999; Jia et al., 2002) and are likely important routes for the entry of synaptically released Zn^{2+} into postsynaptic neurons (Yin et al., 2002; Noh et al., 2005).

To block these channels, we used the selective Ca-AMPA channel blocker NASPM, a synthetic analog of joro spider toxin (Koike et al., 1997; Yin et al., 2002; Noh et al., 2005). Whereas NASPM (100 μM added 10 min before start of OGD) delayed Ca^{2+} deregulation in CA3 pyramidal neurons significantly, it had no effect on the time of Ca^{2+} deregulation in CA1 (Fig. 3*A*). However, because Ca-AMPA channels are permeable to Ca^{2+} as well as Zn^{2+}, we wondered whether inhibition of Ca^{2+} or Zn^{2+} entry was the more important factor in the protective effects of NASPM in CA3. To determine whether the protection provided by NASPM was due to specific blockade of Zn^{2+} entry through Ca-AMPA channels, we made use of mice lacking the vesicular Zn^{2+} transporter ZnT3, which are also completely lacking in presynaptic vesicular Zn^{2+} (Cole et al., 1999). In slices prepared from ZnT3 knock-out mice (ZnT3 KOs), OGD still triggered Zn^{2+} rises and subsequent Ca^{2+} deregulation (data not shown), much as we observed in WT. However, the previously observed protective effects of NASPM, as well as of the Zn^{2+} chelator TPEN, were entirely absent in CA3 neurons of the ZnT3 KOs, strongly arguing that the beneficial effect of NASPM in slices prepared from WT mice was largely due to antagonism of the passage of synaptically released Zn^{2+} through Ca-AMPA channels (Fig. 3*B*). In contrast to the absence of protective effect of TPEN in ZnT3 KOs in CA3, TPEN was still substantially protective in CA1, suggesting that the sources of the Zn^{2+} that contribute to acute OGD-induced injury differ between these hippocampal subzones.

Zn^{2+} mobilization from MT-III contributes to OGD-induced degeneration of CA1 neurons

Observations that Zn^{2+} is stored in presynaptic vesicles and undergoes activity-dependent release and that loss of presynaptic Zn^{2+} occurs concomitantly with Zn^{2+} accumulation in degenerating postsynaptic neurons after ischemia or prolonged seizures led to the expectation that Zn^{2+} "translocation" accounted for the injurious Zn^{2+} accumulation noted to occur in these conditions (Frederickson et al., 1989; Frederickson, 1989; Tønder et al., 1990; Koh et al., 1996). However, using ZnT3 KO mice, the surprising observation was made that, rather than the expected

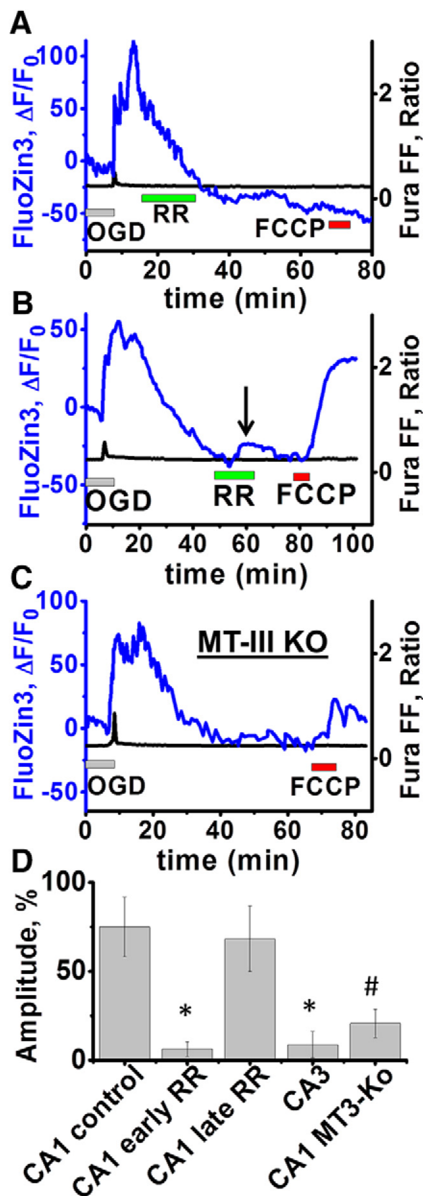

Figure 6. Delayed mitochondrial Zn^{2+} uptake in CA1 pyramidal neurons is substantially attenuated by MCU inhibition shortly after OGD or by deletion of MT-III. CA1 neurons were coloaded with FluoZin-3 and Fura-FF and subjected to sublethal OGD, followed, after 55–60 min (***A***, ***C***) or ~70 min (***B***), by the addition of FCCP (2 μM × 5 min). Traces show the time course of changes in FluoZin-3 $\Delta F/F_0$ (blue) and Fura-FF ratio (black) in representative neurons (mean start times of the initial OGD-evoked Zn^{2+} rise were as follows: ***A***: 7.6 ± 0.6 min, $n = 7$; ***B***: 7.0 ± 0.4 min, $n = 6$; ***C***: 7.1 ± 0.3 min, $n = 10$). ***A***, ***B***, MCU inhibition only blocks mitochondrial Zn^{2+} uptake when applied shortly after OGD, while cytosolic Zn^{2+} is elevated. RR (10 μM for 15 min) was applied ~7–10 min (***A***) or ~35–40 min (***B***) after OGD (traces show representative single neurons), followed by application of FCCP as indicated. Note the absence of FCCP-elicited Zn^{2+} rise with early application of RR, while cytosolic Zn^{2+} was still elevated (***A***), in contrast to the strong FCCP-elicited Zn^{2+} rise with later application of RR (***B***). Also note the small intracellular Zn^{2+} rise triggered by late RR application, most likely resulting from blockage of ongoing Zn^{2+} uptake into mitochondria at this late time point (arrow; seen in 6 of 6 cells examined; mean FCCP-elicited Zn^{2+} rises, as FluoZin-3 $\Delta F/F_0$: ***A***: 6.3 ± 4.2%, $n = 7$, $p = 1.7 \times 10^{-3}$; ***B***: 68 ± 18.3%, $n = 6$, $p = 0.8$; both comparisons with the rise in control, 75 ± 21.9%, from Fig. 5*B*). ***C***, Diminished delayed mitochondrial Zn^{2+} accumulation in CA1 pyramidal neurons of MT-III KO mice. Hippocampal neurons from MT3 mice were loaded with indicators and subjected to sublethal OGD, followed by application of FCCP as in Figure 5*B*. Note the paucity of Zn^{2+} rise triggered by FCCP exposure compared with that seen in WT mice (FluoZin-3 $\Delta F/F_0$: 20.7 ± 8%, $n = 10$). ***D***, Summary data: Delayed mitochondrial Zn^{2+} uptake as a function of treatment. Bars indicate mean FCCP-evoked Zn^{2+} rises (normalized to the pre-FCCP baseline, ΔF_{FCCP}) after sublethal OGD under the conditions indicated. *$p < 0.01$ versus CA1 control; (p-values vs CA1 control are as indicated above: CA1 early RR: $p = 1.7 \times 10^{-3}$; CA1 late RR: $p = 0.8$; CA3: $p = 3.5 \times 10^{-3}$; #for CA1 MT-III KO, we elect not to display a p-value because of the strain difference).

decreases, Zn^{2+} accumulation and damage to CA1 pyramidal neurons were actually increased (Lee et al., 2000). A subsequent study using MT-III KOs and double MT-III/ZnT3 KOs suggested that much of the delayed Zn^{2+} accumulation seen after prolonged seizures in CA1 pyramidal neurons of ZnT-3 KOs was due to Zn^{2+} mobilization from MT-III (Lee et al., 2003).

To assess the contributions of MT-III-bound Zn^{2+} to acute OGD-induced degeneration, we used slices from MT-III KO mice. In these slices, OGD still triggered Zn^{2+} rises and subsequent Ca^{2+} deregulation (data not shown), much as in both WT and ZnT3 KOs. Whereas Zn^{2+} chelation with TPEN delayed Ca^{2+} deregulation in CA3 pyramidal neurons (much as in WT; Fig. 1), the protective effects of TPEN were absent in CA1 neurons of the MT-III KOs (Fig. 4*A*). This strongly suggests that the Zn^{2+} contribution to acute OGD-induced degeneration of CA1 (but not CA3) neurons is mediated largely by Zn^{2+} mobilization from MT-III. Despite the lack of substantial Zn^{2+} contribution to CA1 damage in these mice, Ca^{2+} entry blockers had protective effects in the MT-III KOs similar to those seen in WT slices in both CA1 and CA3 (Fig. 4*B*).

Protracted mitochondrial Zn^{2+} accumulation after sublethal OGD in CA1 but not in CA3 neurons

Whereas above studies highlighted distinct sources of the Zn^{2+} contributing to acute ischemic damage in CA1 versus CA3 pyramidal neurons, we next sought to examine clues to possible differences in targets or effects of the Zn^{2+} after the acute ischemic episode that might help to explain the differential vulnerabilities of CA1 and CA3 neurons in disease conditions. To this aim, we performed OGD of durations just short of those that induced acute Ca^{2+} deregulation and cell death, terminating OGD ~1 min after the onset of the cytosolic Zn^{2+} rise (which generally occurred between 6 and 9 min), and monitored cytosolic Ca^{2+} and Zn^{2+} for an additional 60–80 min. Under these conditions, cytosolic Zn^{2+} rises persisted for ~10–30 min after OGD, followed by recovery over ~40–60 min.

There are several reasons to suspect that mitochondria are important targets for deleterious effects of cytosolic Zn^{2+} accumulation (reviewed in the Discussion). To assess mitochondrial Zn^{2+} accumulation after sublethal OGD exposures, we used the mitochondrial uncoupler FCCP (2 μM, 5 min), which dissipates the proton gradient across the inner mitochondrial membrane, resulting in rapid mitochondrial depolarization (loss of $\Delta\Psi_m$) and release of the Zn^{2+} already present in mitochondria (Sensi et al., 2000; Sensi et al., 2002; Medvedeva et al., 2009; Clausen et al., 2013). Application of FCCP 55–60 min after the end of the OGD episode resulted in a sharp cytosolic Zn^{2+} rise in CA1 neurons, presumably due to the release of Zn^{2+} that had become sequestered in the mitochondria. However, Zn^{2+} responses to identical delayed FCCP treatments were almost absent in CA3 (Fig. 5*A*–*C*). One possible explanation for the absence of a cytosolic Zn^{2+} response to FCCP in CA3 could be that the mitochondria were already fully depolarized at that time and could not sequester Zn^{2+}. To test this, we used the $\Delta\Psi_m$ sensitive indicator Rhod123 to compare $\Delta\Psi_m$ between CA1 and CA3; an increase in fluorescence of this indicator is indicative of loss of $\Delta\Psi_m$. When added 50 min after the end of the OGD, FCCP triggered similar sharp increases in Rhod123 fluorescence (as $\Delta F/F_o$) in both CA1 and CA3 neurons, indicating a similar magnitude of $\Delta\Psi_m$ at

←

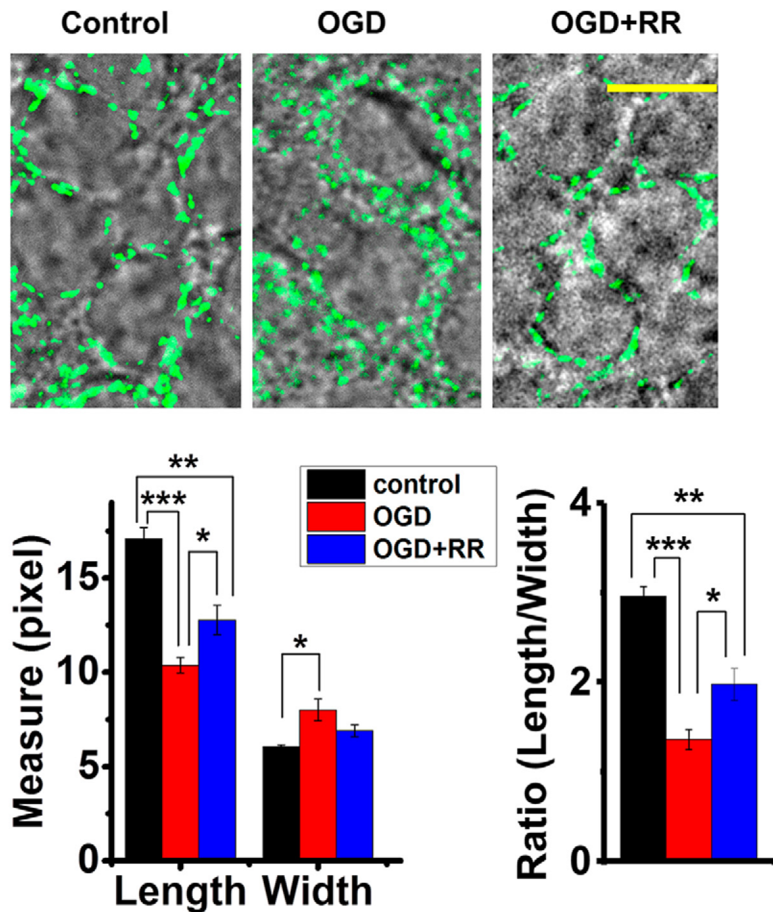

Figure 7. Mitochondrial swelling after OGD in CA1 pyramidal neurons is attenuated by MCU blockade. Brain slices were subjected to sham wash in oxygenated medium (control) or were subjected to 8.5 min OGD either alone or with RR (10 μM, applied 10 min after termination of the OGD for 15 min). One hour after the end of the OGD, slices were fixed (with 4% PFA) and processed for immunostaining with TOM20 antibody. Top, Appearance of mitochondrial swelling. Representative merged images show the bright-field appearance of pyramidal neurons in the CA1 region overlaid with confocal fluorescence images of TOM-20-labeled mitochondria. Scale bar, 10 μm. Bottom, Quantitative measurements. Left, Mitochondrial measurements (length and width; obtained using ImageJ software, see Materials and Methods) after the indicated treatment. Graphs display mean values from 3–5 independently treated hippocampal slices comprising $\geq$18 neurons each condition and with 107 mitochondria measured in control (144 in OGD; 190 in OGD + RR; see Materials and Methods; length of control 1.4 $\pm$ 0.047 μm, OGD 0.8 $\pm$ 0.032 μm, $p = 2.0 \times 10^{-4}$ vs control; OGD + RR 1.0 $\pm$ 0.062 μm, $p = 8 \times 10^{-3}$ vs control, $p = 0.04$ vs OGD; width: control 0.49 $\pm$ 0.007 μm, OGD 0.64 $\pm$ 0.045 μm, $p = 0.03$ vs control; OGD + RR 0.55 $\pm$ 0.024 μm, $p = 0.09$ vs control, $p = 0.1$ vs OGD). Right, Mean L/W ratios observed after each treatment (based on the same data; control 2.9 $\pm$ 0.1, OGD 1.4 $\pm$ 0.11, $p = 1.9 \times 10^{-4}$ vs control; OGD + RR 2.0 $\pm$ 0.17, $p = 7.9 \times 10^{-3}$ vs control, $p = 0.03$ vs OGD). Note that OGD caused a "rounding up" of mitochondria, with a decrease in length and increase in width, and that this change was attenuated by delayed treatment with RR. *$p < 0.05$; **$p < 0.01$; ***$p < 0.001$.

this time point (Fig. 5*D*,*E*). Therefore, the paucity of delayed mitochondrial Zn^{2+} uptake in CA3 does not appear to be explained by greater or more persistent loss of $\Delta\Psi_m$ in these neurons.

Zn^{2+} accumulation in CA1 mitochondria during 'reperfusion' reflects mobilization from MT-III

We next used the MCU blocker RR (Moore, 1971; Medvedeva and Weiss, 2014) to elicit clues as to the time frame during which Zn^{2+} accumulates in the CA1 mitochondria (Fig. 6). When RR was applied for 15 min starting 7–10 min after the end of the OGD (while cytosolic Zn^{2+} levels were still markedly elevated), application of FCCP 30 min later failed to elicit a Zn^{2+} rise (Fig. 6*A*), supporting the hypothesis that much of the Zn^{2+} may have entered the mitochondria during this period of elevated cytosolic Zn^{2+}. As a test of this idea, we also examined the effect of RR application at a later time point (starting ~30–40 min after the end of the OGD), when cytosolic Zn^{2+} rises had largely recovered. With this treatment, subsequent FCCP (15 min after washout of the RR) did result in a large cytosolic Zn^{2+} rise (Fig. 6*B*). The simplest explanation for this observation is that the RR treatment at this later time point largely failed to prevent mitochondrial Zn^{2+} accumulation because considerable Zn^{2+} had already entered the mitochondria, remaining sequestered within them at the time of the FCCP exposure. Notably, however, this delayed RR application caused a small increase in cytosolic Zn^{2+} (Fig. 6*B*, arrow, evident in all six cells examined), supporting the idea that free Zn^{2+} accumulation in the cytosol and its uptake into mitochondria was still ongoing at the indicated time (~40 min after OGD). Finally, to test the contribution of Zn^{2+} mobilization from MT-III to this delayed mitochondrial Zn^{2+} accumulation, we performed an identical sublethal OGD exposure in slices from MT-III KOs. Interestingly, despite the absence of MT-III, we still saw cytosolic Zn^{2+} rises that persisted for a period of 10–20 min after the end of the OGD. However, upon delayed application of FCCP, cytosolic Zn^{2+} rises were considerably less than in WT (Fig. 6*C*).

Mitochondrial swelling after OGD in CA1 pyramidal neurons is attenuated by MCU blockade

Finally, to examine a possible consequence of the mitochondrial Zn^{2+} uptake in CA1, we used confocal imaging to assess changes in mitochondrial morphology ~1 h after sublethal OGD. Slices were exposed either to sham wash in oxygenated medium (as a control) or to a sublethal (~8.5 min) episode of OGD either alone or with RR applied 10 min after the end of the OGD for 15 min (as in Fig. 6*A*, top). One hour after OGD, slices were fixed and immunolabeled with antibody for the mitochondrial outer membrane marker TOM20. Slices were examined under confocal microscopy (1000×) and images were obtained in the CA1 pyramidal layer (Fig. 7, top). For quantitative assessment, images were adjusted using ImageJ software to discriminate mitochondrial borders from background optimally and perinuclear regions were cropped from images and coded for blinded measurement of mitochondrial lengths and widths (see Materials and Methods). We found that OGD caused a marked "rounding up" of the mitochondria, with substantial decreases in their mean lengths, increases in their widths, and decreased length/width (L/W) ratios. We further found that delayed application of RR attenuated this effect, yielding an intermediate L/W ratio (Fig. 7, bottom).

Discussion

Distinct 'pools' contribute to injurious hippocampal Zn^{2+} accumulation *in vivo*

Despite high (>100 μM) levels of Zn^{2+} in the brain, under resting conditions, it is almost all sequestered, such that free levels are

very low (generally <1 nM; Frederickson, 1989). One major site of Zn^{2+} sequestration is in synaptic vesicles, where it is stored via action of the vesicular Zn^{2+} transporter ZnT3 (Cole et al., 1999) and undergoes activity-dependent release (Assaf and Chung, 1984; Howell et al., 1984). Observations of Zn^{2+} accumulation in injured and degenerating neurons after prolonged seizures or ischemia (Frederickson et al., 1989; Tønder et al., 1990) led to the proposition that "Zn^{2+} translocation" across the synapse might contribute critically to the associated neurodegeneration. The link between Zn^{2+} accumulation and neurodegeneration was strengthened markedly by observations that the extracellular Zn^{2+} chelator Ca-EDTA was highly protective in ischemia (Koh et al., 1996; Calderone et al., 2004). Studies of Zn^{2+} entry routes indicated permeation through VGCC, with particular rapidity through Ca-AMPA channels (Weiss et al., 1993; Yin and Weiss, 1995; Sensi et al., 1999; Jia et al., 2002). Indeed, Zn^{2+} entry through Ca-AMPA channels appears to contribute to ischemic injury both acutely and at delayed time points after transient ischemia, after numbers of these channels have been upregulated (Yin et al., 2002; Noh et al., 2005).

The generation of ZnT3 KO mice provided a model to examine directly the specific contribution of synaptic Zn^{2+} release in neurodegeneration (Cole et al., 1999). Surprisingly, ZnT3 knock-out actually increased the delayed Zn^{2+} accumulation and neuronal injury occurring after prolonged kainate seizures in CA1 neurons (while modestly decreasing them in CA3; Lee et al., 2000). It subsequently became apparent that another important Zn^{2+} pool is that which is bound to Zn^{2+}-buffering proteins such as MTs (MT-III being the primary isoform in neurons). Studies in neuronal culture revealed that strong Zn^{2+} mobilization from these proteins in the absence of any extracellular Zn^{2+} entry could trigger Zn^{2+}-dependent neuronal injury (Aizenman et al., 2000; Bossy-Wetzel et al., 2004), and also indicated that, depending upon conditions, MT-III could either provide a source of Zn^{2+} that could injure neurons upon mobilization or a buffer that could provide protection from cytosolic Zn^{2+} loads (Malaiyandi et al., 2004). The generation of MT-III KOs provided a model to examine directly its roles *in vivo* (Erickson et al., 1997). Interestingly, MT-III appeared to act in both of these ways, with the knock-out decreasing Zn^{2+} accumulation and injury in CA1 while increasing injury in CA3 after prolonged kainate seizure, consistent with its being a source of injurious Zn^{2+} in CA1, but buffering incoming Zn^{2+} loads to provide protection in CA3 (Erickson et al., 1997; Lee et al., 2003). Present studies extend these *in vivo* studies by revealing distinct sources and dynamics of injurious Zn^{2+} accumulation in CA1 and CA3 neurons in acute ischemic injury with acute entry of synaptic Zn^{2+} via Ca-AMPA channels dominating in CA3 and rapid and ongoing mobilization from MT-III appearing to dominate in CA1.

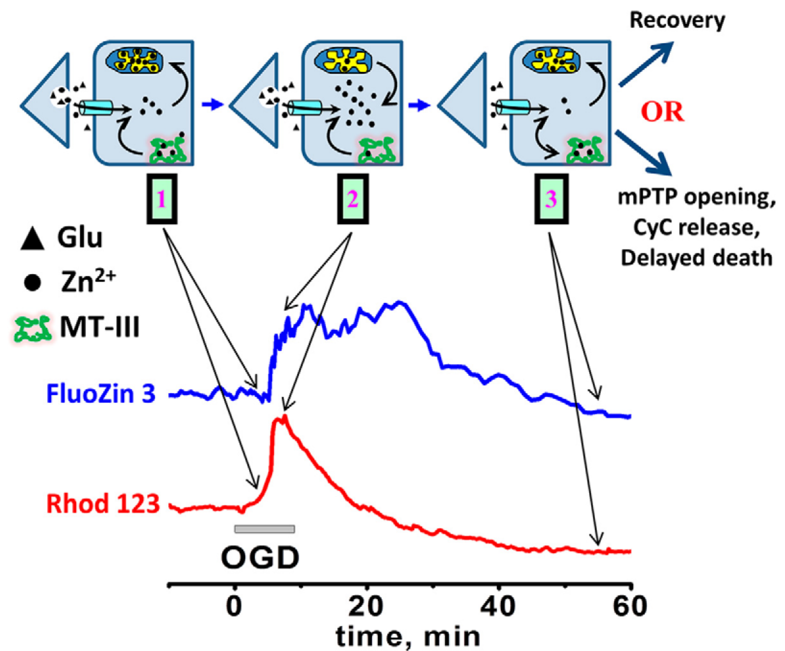

Figure 8. Schematic model showing possible acute and early "reperfusion" events after sublethal ischemia in CA1 pyramidal neurons. Traces show representative FluoZin-3 changes from a single neuron and Rhod123 changes from the CA1 pyramidal cell layer of a different slice. (1) Early OGD: Zn^{2+} (circles) and glutamate (triangles) are released from presynaptic terminals. Zn^{2+} and Ca^{2+} enter postsynaptic neurons via glutamate activated (Ca-AMPA and NMDA) channels and VGCC. Zn^{2+} is also mobilized from MT-III as a result of ischemia-associated oxidative stress and acidosis. Intracellular Zn^{2+} and Ca^{2+} are taken up by mitochondria (via the MCU). Mitochondrial dysfunction including ROS generation will promote further Zn^{2+} mobilization, resulting in a feed-forward cascade of mitochondrial dysfunction and Zn^{2+} accumulation. This uptake causes early mitochondrial depolarization (loss of $\Delta\Psi_m$), which precedes the sharp cytosolic Zn^{2+} rise. (2) Later during OGD, after some threshold of mitochondrial Zn^{2+} and Ca^{2+} accumulation, mitochondria strongly depolarize (loss of $\Delta\Psi_m$) and the Zn^{2+} and Ca^{2+} sequestered within them are released back into the cytosol. At this point, the oxidative and acidotic environment combined with mitochondrial dysfunction will impair both the buffering of Zn^{2+} by MT-III and cellular extrusion of Ca^{2+} and Zn^{2+}, impeding recovery of ionic homeostasis. In the absence of prompt reperfusion, severe cytosolic Ca^{2+} deregulation and rapid cell death ensues. (3) "Reperfusion" after sublethal OGD: if reperfusion with restoration of O_2 and glucose occurs before the onset of Ca^{2+} deregulation, then mitochondria can begin to recover function and $\Delta\Psi_m$. With recovery of $\Delta\Psi_m$ (along with oxidative environment possibly worsened by reperfusion), cytosolic Zn^{2+} is taken back up into mitochondria, where it can remain sequestered for extended periods of time (likely hours; Sensi et al., 2002; Bonanni et al., 2006) and can impair their function (likely synergistically with Ca^{2+}; Sensi et al., 2000; Jiang et al., 2001). Depending upon the extent of Zn^{2+} uptake, mitochondria might gradually recover their normal function or may undergo delayed dysfunction comprising ROS production and opening of the mPTP, with the release of cytochrome C (CyC) and other apoptotic mediators, contributing to delayed cell death. Such a mechanism is compatible with findings of preferential delayed mitochondrial dysfunction with CyC release in CA1 pyramidal neurons after transient ischemia (Nakatsuka et al., 1999; Sugawara et al., 1999).

Mitochondria as critical targets of injurious Zn^{2+} effects

Whereas past studies have highlighted several mechanisms through which Zn^{2+} mediates neurotoxic effects, we and others have found Zn^{2+} to disrupt mitochondrial function potently *in vitro* (Weiss et al., 2000; Dineley et al., 2003; Shuttleworth and Weiss, 2011), causing dose-dependent mitochondrial dysfunction that correlates well with the extent of injury evolving over the subsequent hours, leading us to hypothesize that mitochondria may be a key locus of its neurotoxic effects. Zn^{2+} appears to enter the mitochondria through the MCU (Saris and Niva, 1994; Jiang et al., 2001; Malaiyandi et al., 2005; Gazaryan et al., 2007; Medvedeva and Weiss, 2014) and to affect their function with far greater potency than Ca^{2+}, causing mitochondrial depolarization, ROS generation, and potent induction of swelling, probably due to activation of a large conductance channel, the mitochondrial permeability transition pore (mPTP; Wudarczyk et al., 1999; Jiang et al., 2001; Gazaryan et al., 2007).

Despite the high potency of its effects on isolated mitochondria, relatively high extracellular Zn^{2+} exposures are needed to disrupt mitochondrial function potently in intact neurons under resting conditions, raising questions as to the degree of mitochondrial dysfunction and injury likely to be triggered by presynaptic Zn^{2+} release and its translocation into postsynaptic neurons (Pivovarova et al., 2014). However, cytosolic buffering (by MTs or related peptides) is normally highly protective from cytosolic Zn^{2+} loads and, under disease-associated conditions of oxidative stress and/or acidosis, buffering is impaired and mitochondrial Zn^{2+} uptake and disruption of function can occur with far lower levels or even in the absence of extracellular Zn^{2+} (Sensi et al., 2003; Clausen et al., 2013). Indeed, intracellular mobilization and accumulation of endogenous Zn^{2+} can affect mitochondrial function both in neuronal cultures (Sensi et al., 2003; Bossy-Wetzel et al., 2004), and in postischemic hippocampus (Calderone et al., 2004; Bonanni et al., 2006). Furthermore, our recent slice studies strongly support the idea that specific entry of endogenous Zn^{2+} into mitochondria through the MCU contributes to ROS generation and injury during acute OGD (Medvedeva and Weiss, 2014).

Notably, mitochondria seem to be critically involved in the delayed selective degeneration of CA1 pyramidal neurons after transient ischemia. These neurons show mitochondrial swelling with release of cytochrome C into the cytosol beginning within hours of ischemia, before caspase-3 activation and with the appearance of TUNEL-positive cells and neurodegeneration with prominent DNA fragmentation occurring over several days (Antonawich, 1999; Nakatsuka et al., 1999; Ouyang et al., 1999; Sugawara et al., 1999). In addition, early treatment with either the Zn^{2+} chelator Ca-EDTA (Calderone et al., 2004) or the mPTP blocker cyclosporine A (CsA; Nakatsuka et al., 1999) decreased delayed cytochrome C release in CA1 neurons after ischemia, supporting contributory roles of Zn^{2+} and the mPTP to the activation of this apoptotic pathway. In light of the potent effects of Zn^{2+} on mitochondria, we propose that the protracted Zn^{2+} accumulation that we found here to occur selectively in mitochondria of CA1 neurons represents a critical early and targetable event in the cascade of events culminating in the delayed selective degeneration of CA1 neurons.

Summary and therapeutic implications

Whereas *in vivo* studies have examined Zn^{2+} effects on outcome hours to days after the ischemic event, its contributions to the initiation of death cascades have been relatively little studied. The present study used an acute hippocampal slice model of ischemia, which provides the benefit of enabling real-time high-resolution tracking of changes to assess differences in Ca^{2+}- and Zn^{2+}-dependent excitotoxic triggering events between CA1 and CA3 pyramidal neurons that may bear upon their differential susceptibilities. Our findings suggest that rapid excitotoxic Ca^{2+} and Zn^{2+} entry may dominate in CA3, possibly consistent with the particular susceptibility of these neurons after recurrent limbic seizures, which are characterized by repetitive firing of Zn^{2+} rich mossy fiber terminals. However, in the case of a sublethal insult, CA3 neurons may be better able to recover ionic homeostasis. In contrast to the dominant role of acute Zn^{2+} translocation through Ca-AMPA channels in CA3, Zn^{2+} mobilization from MT-III appears to dominate in CA1. Notably, mobilization from MT-III also appears to underlie ongoing Zn^{2+} accumulation in CA1 mitochondria during the "reperfusion" phase, well after the end of sublethal episodes of OGD. We suggest that this ongoing Zn^{2+} accumulation in CA1 mitochondria is integral to the delayed activation of apoptotic injury in CA1, with sequential occurrence of ROS generation, mitochondrial swelling due to mPTP activation, cytochrome C release, and caspase activation contributing to delayed cell death.

Elucidation of these early excitotoxic events in CA1 versus CA3 pyramidal neurons may have therapeutic implications. In the case of acute neuronal injury resulting from prolonged seizures or ischemia, anti-excitotoxic interventions, including specific blockage of Ca-AMPA channels, may be of particular utility in CA3. In contrast, whereas acute excitotoxic ion entry certainly contributes in CA1, interventions aiming to attenuate Zn^{2+} accumulation in mitochondria (and downstream consequences thereof) may be of particular value both acutely and after sublethal insults to diminish delayed injury. Potential interventions could include MCU blockers to attenuate delayed mitochondrial Zn^{2+} accumulation (although, depending upon conditions, they also have potential to exacerbate cytosolic Ca^{2+} loading; Velasco and Tapia, 2000; Medvedeva and Weiss, 2014), antioxidants (which may attenuate oxidation dependent Zn^{2+} release from MT-III), or mPTP blockers such as CsA that should attenuate downstream mPTP activation (Uchino et al., 1998; Nakatsuka et al., 1999; Friberg and Wieloch, 2002). Indeed, in light of the complexity of the events leading to delayed degeneration, it is likely that no single intervention will be optimal, but that combinations of interventions, likely delivered in distinct temporal phases of the injury cascade, will provide the best outcome. We hope that further clarification of early Zn^{2+}-related events in CA1 versus CA3 pyramidal neurons in a model of ischemia will ultimately aid the development of targeted treatments to diminish injury to these vulnerable neuronal populations after ischemia or recurrent seizures.

Notes

Supplemental material for this article is available at https://doi.org/10.5281/zenodo.168248. The posted data provide the control characterization of the OGD-triggered occurrences of cytosolic Zn^{2+} rises and terminal Ca^{2+} deregulation events in individual CA1 and CA3 pyramidal neurons in acute hippocampal slices of MT-III knock-out mice (004649-129S7-Mt3tm1Rpa/J; Jackson Laboratory) and ZnT3 knock-out mice (005064-B6;129-Slc30a3tm1Rpa/J; Jackson Laboratory) that are used in these studies. This material has not been peer reviewed.

References

Aizenman E, Stout AK, Hartnett KA, Dineley KE, McLaughlin B, Reynolds IJ (2000) Induction of neuronal apoptosis by thiol oxidation: putative role of intracellular zinc release. J Neurochem 75:1878–1888. Medline

Antonawich FJ (1999) Translocation of cytochrome c following transient global ischemia in the gerbil. Neurosci Lett 274:123–126. CrossRef Medline

Assaf SY, Chung SH (1984) Release of endogenous Zn2+ from brain tissue during activity. Nature 308:734–736. CrossRef Medline

Ben-Ari Y, Tremblay E, Ottersen OP (1980a) Injections of kainic acid into the amygdaloid complex of the rat: an electrographic, clinical and histological study in relation to the pathology of epilepsy. Neuroscience 5: 515–528. CrossRef Medline

Ben-Ari Y, Tremblay E, Ottersen OP, Meldrum BS (1980b) The role of epileptic activity in hippocampal and "remote" cerebral lesions induced by kainic acid. Brain Res 191:79–97. CrossRef Medline

Bonanni L, Chachar M, Jover-Mengual T, Li H, Jones A, Yokota H, Ofengeim D, Flannery RJ, Miyawaki T, Cho CH, Polster BM, Pypaert M, Hardwick JM, Sensi SL, Zukin RS, Jonas EA (2006) Zinc-dependent multi-conductance channel activity in mitochondria isolated from ischemic brain. J Neurosci 26:6851–6862. CrossRef Medline

Bossy-Wetzel E, Talantova MV, Lee WD, Schölzke MN, Harrop A, Mathews E, Götz T, Han J, Ellisman MH, Perkins GA, Lipton SA (2004) Crosstalk between nitric oxide and zinc pathways to neuronal cell death involving mitochondrial dysfunction and p38-activated K(+) channels. Neuron 41:351–365. CrossRef Medline

Calderone A, Jover T, Mashiko T, Noh KM, Tanaka H, Bennett MV, Zukin RS (2004) Late calcium EDTA rescues hippocampal CA1 neurons from global ischemia-induced death. J Neurosci 24:9903–9913. CrossRef Medline

Choi DW (1987) Ionic dependence of glutamate neurotoxicity. J Neurosci 7:369–379. Medline

Clausen A, McClanahan T, Ji SG, Weiss JH (2013) Mechanisms of rapid reactive oxygen species generation in response to cytosolic Ca2+ or Zn2+ loads in cortical neurons. PLoS One 8:e83347. CrossRef Medline

Cole TB, Wenzel HJ, Kafer KE, Schwartzkroin PA, Palmiter RD (1999) Elimination of zinc from synaptic vesicles in the intact mouse brain by disruption of the ZnT3 gene. Proc Natl Acad Sci U S A 96:1716–1721. CrossRef Medline

Dineley KE, Votyakova TV, Reynolds IJ (2003) Zinc inhibition of cellular energy production: implications for mitochondria and neurodegeneration. J Neurochem 85:563–570. CrossRef Medline

Duchen MR, Surin A, Jacobson J (2003) Imaging mitochondrial function in intact cells. Methods Enzymol 361:353–389. CrossRef Medline

Erickson JC, Hollopeter G, Thomas SA, Froelick GJ, Palmiter RD (1997) Disruption of the metallothionein-III gene in mice: analysis of brain zinc, behavior, and neuron vulnerability to metals, aging, and seizures. J Neurosci 17:1271–1281. Medline

Frederickson CJ (1989) Neurobiology of zinc and zinc-containing neurons. Int Rev Neurobiol 31:145–238. CrossRef Medline

Frederickson CJ, Hernandez MD, McGinty JF (1989) Translocation of zinc may contribute to seizure-induced death of neurons. Brain Res 480:317–321. CrossRef Medline

Friberg H, Wieloch T (2002) Mitochondrial permeability transition in acute neurodegeneration. Biochimie 84:241–250. CrossRef Medline

Gazaryan IG, Krasinskaya IP, Kristal BS, Brown AM (2007) Zinc irreversibly damages major enzymes of energy production and antioxidant defense prior to mitochondrial permeability transition. J Biol Chem 282:24373–24380. CrossRef Medline

Hollmann M, Hartley M, Heinemann S (1991) Ca2+ permeability of KA-AMPA-gated glutamate receptor channels depends on subunit composition. Science 252:851–853. CrossRef Medline

Howell GA, Welch MG, Frederickson CJ (1984) Stimulation-induced uptake and release of zinc in hippocampal slices. Nature 308:736–738. CrossRef Medline

Jia Y, Jeng JM, Sensi SL, Weiss JH (2002) Zn2+ currents are mediated by calcium-permeable AMPA/kainate channels in cultured murine hippocampal neurones. J Physiol 543:35–48. CrossRef Medline

Jiang D, Sullivan PG, Sensi SL, Steward O, Weiss JH (2001) Zn(2+) induces permeability transition pore opening and release of pro-apoptotic peptides from neuronal mitochondria. J Biol Chem 276:47524–47529. CrossRef Medline

Kirino T (1982) Delayed neuronal death in the gerbil hippocampus following ischemia. Brain Res 239:57–69. CrossRef Medline

Koh JY, Suh SW, Gwag BJ, He YY, Hsu CY, Choi DW (1996) The role of zinc in selective neuronal death after transient global cerebral ischemia. Science 272:1013–1016. CrossRef Medline

Koike M, Iino M, Ozawa S (1997) Blocking effect of 1-naphthyl acetyl spermine on Ca(2+)-permeable AMPA receptors in cultured rat hippocampal neurons. Neurosci Res 29:27–36. CrossRef Medline

Lee JY, Cole TB, Palmiter RD, Koh JY (2000) Accumulation of zinc in degenerating hippocampal neurons of ZnT3-null mice after seizures: evidence against synaptic vesicle origin. J Neurosci 20:RC79. Medline

Lee JY, Kim JH, Palmiter RD, Koh JY (2003) Zinc released from metallothionein-iii may contribute to hippocampal CA1 and thalamic neuronal death following acute brain injury. Exp Neurol 184:337–347. CrossRef Medline

Lerma J, Morales M, Ibarz JM, Somohano F (1994) Rectification properties and Ca2+ permeability of glutamate receptor channels in hippocampal cells. Eur J Neurosci 6:1080–1088. CrossRef Medline

Malaiyandi LM, Dineley KE, Reynolds IJ (2004) Divergent consequences arise from metallothionein overexpression in astrocytes: zinc buffering and oxidant-induced zinc release. Glia 45:346–353. CrossRef Medline

Malaiyandi LM, Vergun O, Dineley KE, Reynolds IJ (2005) Direct visualization of mitochondrial zinc accumulation reveals uniporter-dependent and -independent transport mechanisms. J Neurochem 93:1242–1250. CrossRef Medline

Medvedeva YV, Weiss JH (2014) Intramitochondrial Zn(2+) accumulation via the Ca(2+) uniporter contributes to acute ischemic neurodegeneration. Neurobiol Dis 68:137–144. CrossRef Medline

Medvedeva YV, Lin B, Shuttleworth CW, Weiss JH (2009) Intracellular Zn2+ accumulation contributes to synaptic failure, mitochondrial depolarization, and cell death in an acute slice oxygen-glucose deprivation model of ischemia. J Neurosci 29:1105–1114. CrossRef Medline

Moore CL (1971) Specific inhibition of mitochondrial Ca++ transport by ruthenium red. Biochem Biophys Res Commun 42:298–305. CrossRef Medline

Nakatsuka H, Ohta S, Tanaka J, Toku K, Kumon Y, Maeda N, Sakanaka M, Sakaki S (1999) Release of cytochrome c from mitochondria to cytosol in gerbil hippocampal CA1 neurons after transient forebrain ischemia. Brain Res 849:216–219. CrossRef Medline

Noh KM, Yokota H, Mashiko T, Castillo PE, Zukin RS, Bennett MV (2005) Blockade of calcium-permeable AMPA receptors protects hippocampal neurons against global ischemia-induced death. Proc Natl Acad Sci U S A 102:12230–12235. CrossRef Medline

Ogoshi F, Weiss JH (2003) Heterogeneity of Ca2+-permeable AMPA/kainate channel expression in hippocampal pyramidal neurons: fluorescence imaging and immunocytochemical assessment. J Neurosci 23:10521–10530. Medline

Ordy JM, Wengenack TM, Bialobok P, Coleman PD, Rodier P, Baggs RB, Dunlap WP, Kates B (1993) Selective vulnerability and early progression of hippocampal CA1 pyramidal cell degeneration and GFAP-positive astrocyte reactivity in the rat four-vessel occlusion model of transient global ischemia. Exp Neurol 119:128–139. CrossRef Medline

Ouyang YB, Tan Y, Comb M, Liu CL, Martone ME, Siesjö BK, Hu BR (1999) Survival- and death-promoting events after transient cerebral ischemia: phosphorylation of Akt, release of cytochrome C and Activation of caspase-like proteases. J Cereb Blood Flow Metab 19:1126–1135. Medline

Petito CK, Feldmann E, Pulsinelli WA, Plum F (1987) Delayed hippocampal damage in humans following cardiorespiratory arrest. Neurology 37:1281–1286. CrossRef Medline

Pivovarova NB, Stanika RI, Kazanina G, Villanueva I, Andrews SB (2014) The interactive roles of zinc and calcium in mitochondrial dysfunction and neurodegeneration. J Neurochem 128:592–602. CrossRef Medline

Randall RD, Thayer SA (1992) Glutamate-induced calcium transient triggers delayed calcium overload and neurotoxicity in rat hippocampal neurons. J Neurosci 12:1882–1895. Medline

Rothman SM, Olney JW (1986) Glutamate and the pathophysiology of hypoxic-ischemic brain damage. Ann Neurol 19:105–111. CrossRef Medline

Saris NE, Niva K (1994) Is Zn2+ transported by the mitochondrial calcium uniporter? FEBS Lett 356:195–198. CrossRef Medline

Sensi SL, Yin HZ, Carriedo SG, Rao SS, Weiss JH (1999) Preferential Zn2+ influx through Ca2+-permeable AMPA/kainate channels triggers prolonged mitochondrial superoxide production. Proc Natl Acad Sci U S A 96:2414–2419. CrossRef Medline

Sensi SL, Yin HZ, Weiss JH (2000) AMPA/kainate receptor-triggered Zn2+ entry into cortical neurons induces mitochondrial Zn2+ uptake and persistent mitochondrial dysfunction. Eur J Neurosci 12:3813–3818. CrossRef Medline

Sensi SL, Ton-That D, Weiss JH (2002) Mitochondrial sequestration and Ca(2+)-dependent release of cytosolic Zn(2+) loads in cortical neurons. Neurobiol Dis 10:100–108. CrossRef Medline

Sensi SL, Ton-That D, Sullivan PG, Jonas EA, Gee KR, Kaczmarek LK, Weiss JH (2003) Modulation of mitochondrial function by endogenous Zn2+ pools. Proc Natl Acad Sci U S A 100:6157–6162. CrossRef Medline

Shuttleworth CW, Weiss JH (2011) Zinc: new clues to diverse roles in brain ischemia. Trends Pharmacol Sci 32:480–486. CrossRef Medline

Siesjö BK (1988) Historical overview: calcium, ischemia, and death of brain cells. Ann N Y Acad Sci 522:638–661. CrossRef Medline

Stork CJ, Li YV (2006) Intracellular zinc elevation measured with a "calcium-specific" indicator during ischemia and reperfusion in rat hippocampus: a question on calcium overload. J Neurosci 26:10430–10437. CrossRef Medline

Sugawara T, Fujimura M, Morita-Fujimura Y, Kawase M, Chan PH (1999) Mitochondrial release of cytochrome c corresponds to the selective vulnerability of hippocampal CA1 neurons in rats after transient global cerebral ischemia. J Neurosci 19:RC39. Medline

Tanaka S, Kondo S, Tanaka T, Yonemasu Y (1988) Long-term observation of rats after unilateral intra-amygdaloid injection of kainic acid. Brain Res 463:163–167. CrossRef Medline

Tønder N, Johansen FF, Frederickson CJ, Zimmer J, Diemer NH (1990) Possible role of zinc in the selective degeneration of dentate hilar neurons

after cerebral ischemia in the adult rat. Neurosci Lett 109:247–252. CrossRef Medline

Uchino H, Elmér E, Uchino K, Li PA, He QP, Smith ML, Siesjö BK (1998) Amelioration by cyclosporin A of brain damage in transient forebrain ischemia in the rat. Brain Res 812:216 –226. CrossRef Medline

Vander Jagt TA, Connor JA, Shuttleworth CW (2008) Localized loss of Ca2+ homeostasis in neuronal dendrites is a downstream consequence of metabolic compromise during extended NMDA exposures. J Neurosci 28:5029 –5039. CrossRef Medline

Velasco I, Tapia R (2000) Alterations of intracellular calcium homeostasis and mitochondrial function are involved in ruthenium red neurotoxicity in primary cortical cultures. J Neurosci Res 60:543–551. CrossRef Medline

Verdoorn TA, Burnashev N, Monyer H, Seeburg PH, Sakmann B (1991) Structural determinants of ion flow through recombinant glutamate receptor channels. Science 252:1715–1718. CrossRef Medline

Wei G, Hough CJ, Li Y, Sarvey JM (2004) Characterization of extracellular accumulation of Zn2+ during ischemia and reperfusion of hippocampus slices in rat. Neuroscience 125:867– 877. CrossRef Medline

Weiss JH, Hartley DM, Koh JY, Choi DW (1993) AMPA receptor activation potentiates zinc neurotoxicity. Neuron 10:43– 49. CrossRef Medline

Weiss JH, Sensi SL, Koh JY (2000) Zn(2+): a novel ionic mediator of neural injury in brain disease. Trends Pharmacol Sci 21:395– 401. CrossRef Medline

Wudarczyk J, Debska G, Lenartowicz E (1999) Zinc as an inducer of the membrane permeability transition in rat liver mitochondria. Arch Biochem Biophys 363:1– 8. CrossRef Medline

Yin HZ, Weiss JH (1995) Zn(2+) permeates Ca(2+) permeable AMPA/kainate channels and triggers selective neural injury. Neuroreport 6:2553–2556. CrossRef Medline

Yin HZ, Sensi SL, Carriedo SG, Weiss JH (1999) Dendritic localization of Ca(2+)-permeable AMPA/kainate channels in hippocampal pyramidal neurons. J Comp Neurol 409:250 –260. Medline

Yin HZ, Sensi SL, Ogoshi F, Weiss JH (2002) Blockade of Ca2+-permeable AMPA/kainate channels decreases oxygen-glucose deprivation-induced Zn2+ accumulation and neuronal loss in hippocampal pyramidal neurons. J Neurosci 22:1273–1279. Medline

Zola-Morgan S, Squire LR, Amaral DG (1986) Human amnesia and the medial temporal region: enduring memory impairment following a bilateral lesion limited to field CA1 of the hippocampus. J Neurosci 6:2950 – 2967. Medline